Hydrol. Earth Syst. Sci. Discuss., 12, 9813–9864, 2015
www.hydrol-earth-syst-sci-discuss.net/12/9813/2015/
doi:10.5194/hessd-12-9813-2015

Hydrology and Earth System Sciences
Open Access
Discussions

Use of cosmic ray neutron sensors for soil moisture monitoring in forests

I. Heidbüchel, A. Güntner, and T. Blume

GFZ German Research Centre for Geosciences, Helmholtz Centre, Potsdam, Germany

Received: 23 August 2015 – Accepted: 2 September 2015 – Published: 25 September 2015

Correspondence to: I. Heidbüchel (ingo.heidbuechel@gfz-potsdam.de)

Published by Copernicus Publications on behalf of the European Geosciences Union.

Abstract

Cosmic ray neutron sensors (CRS) are a promising technique to measure soil moisture at intermediate scales. To convert neutron counts to average volumetric soil water content a simple calibration function can be used (the N_0-calibration of Desilets et al., 2010). This calibration function is based on soil water content derived directly from soil samples taken within the footprint of the sensor. We installed a CRS in a mixed forest in the lowlands of north-eastern Germany and calibrated it 10 times throughout one calendar year. Each calibration with the N_0-calibration function resulted in a different CRS soil moisture time series, with deviations of up to $0.12\,m^3\,m^{-3}$ for individual values of soil water content. Also, many of the calibration efforts resulted in time series that could not be matched with independent in situ measurements of soil water content. We therefore suggest a new calibration function with a different shape that can vary from one location to another. A two-point calibration proved to be adequate to correctly define the shape of the new calibration function if the calibration points were taken during both dry and wet conditions covering at least 50 % of the total range of soil moisture. The best results were obtained when the soil samples used for calibration were linearly weighted as a function of depth in the soil profile and non-linearly weighted as a function of distance from the CRS, and when the depth-specific amount of soil organic matter and lattice water content was explicitly considered. The annual cycle of tree foliation was found to be a negligible factor for calibration because the variable hydrogen mass in the leaves was small compared to the hydrogen mass changes by soil moisture variations. Finally, we provide a best practice calibration guide for CRS in forested environments.

1 Introduction

Measuring soil moisture comprehensively over larger areas is difficult, mainly for two reasons. Firstly, soil moisture can be highly variable ~~already~~ at small scales, especially

HESSD
12, 9813–9864, 2015

under dry conditions (e.g. Western et al., 2004). Secondly, most common in situ measurement techniques only yield point measurements. To obtain a valid estimate of average soil moisture one needs to collect data from numerous locations within a given area. This can be very cumbersome. More recently, remote sensing of soil moisture at larger scales has become a research focus (e.g. see Ochsner et al., 2013 for a recent review); however, ~~up to this point~~ the measurement depth of many of these methods is still limited to the upper 5 cm of the soil. Also, both spatial and temporal resolution is rather coarse. A technique that intends to bridge the scale gap between point measurements of soil moisture and remote sensing is the use of cosmic ray neutrons as indicators of soil moisture. A detailed description of the functioning of the cosmic ray neutron sensors (CRS) can be found in Zreda et al. (2008, 2012), here we will only describe the basic measurement principle. Cosmic ray neutrons are formed when high-energy cosmic ray particles deriving from the sun (and also from other galaxies) enter the Earth's atmosphere. Once there, they start interacting with other atomic nuclei producing cascades of fast neutrons (that are also called low-energy neutrons) that travel towards the Earth's surface and into the soils. The number of fast neutrons above the soil surface depends strongly on the number of hydrogen atoms in the surroundings because hydrogen atoms have a very high capacity to moderate fast cosmic ray neutrons (that means to slow them down and turn them into thermal neutrons with even less energy – effectively removing the fast neutrons from the system). The number of hydrogen atoms increases with increasing soil water content and hence soils with high water contents re-emit fewer fast neutrons than soils with low water content. That leads to fewer fast neutrons being detected above-ground by the CRS which is generally installed 1–2 m above the soil surface.

Already in 1966 Hendrick and Edge reported that the intensity of fast (low-energy) neutrons (~ 1 keV) detected ~~above-ground~~ depended on the hydrogen content of the soil, and Kodama (1985) found an inverse correlation of neutron intensity and soil moisture content. In 2008, Zreda et al. introduced a method to measure average soil water content over a ~~larger~~ area with CRS. The footprint of CRS, i.e. the area around

HESSD
12, 9813–9864, 2015

the sensor where 86 % of detected neutrons originate from, covers a circle with an approximate radius of 300 m (Desilets and Zreda, 2013). However, the radius can decrease with increasing air density and humidity, with increasing vegetation density and with increasing soil moisture to about 100 m (Köhli et al., 2015). The critical depth of CRS, i.e. the soil depth where 86 % of detected neutrons originate from, varies between 10 and 70 cm below surface (Franz et al., 2012a), depending on soil type, water content and distance from the sensor. Different depth-weighting approaches have been proposed, some of them assuming a linear decrease of weights with depth (Franz et al., 2012a), others assuming a non-linear decrease with depth (Köhli et al., 2015).

The original measurement method uses a relationship between neutron flux and volumetric soil water content with the shape of the relationship being known from neutron transport simulations. For this relationship, Desilets et al. (2010) presented an equation with three constant shape parameters (a_0, a_1, a_2) and one calibration parameter (N_0) which has to be calibrated with soil moisture values determined by the gravimetric method from field soil samples. The influence of soil lattice water and soil organic matter on the signal was investigated by Zreda et al. (2012). They found that both lattice water and soil organic matter contain fixed amounts of hydrogen that further attenuate the neutron signal and need to be taken into account. Lattice water and soil organic matter corrections to the original relationship by Desilets et al. (2010) are provided e.g. in Lv et al. (2014). Other external factors influencing the neutron count that need to be corrected for are (a) atmospheric pressure (Bachelet et al., 1965), (b) incoming neutron flux (see e.g. Bogena et al., 2013) and (c) specific humidity (Rosolem et al., 2013). More recently, the effects of living biomass on the neutron signal have been discussed. Bogena et al. (2013) noted that aboveground biomass reduced the neutron count rate and thus decreased the sensitivity of the sensor. To counter this loss of sensitivity they recommended a 24 h integration time for their forested catchment as a compromise between decreased uncertainty and decreased time resolution. Hawdon et al. (2013) compared neutron counts for locations with different amounts of biomass

HESSD
12, 9813–9864, 2015

and reported that the variation in biomass could explain 80 % of the variation in neutron counts when assuming a nonlinear relationship between biomass and neutron counts. Baatz et al. (2015) also related biomass to neutron counts, but proposed a linear relationship between the two variables. Baroni and Oswald (2015) suggested that the influence of above-ground biomass between the sensor and the ground which decreases the critical depth of the CRS can be incorporated into the weighting approach of Franz et al. (2012a). Coopersmith et al. (2014) found that soil moisture in a corn crop is often overestimated when the leaf area index (LAI) is relatively high while it is underestimated when LAI is relatively low – circumstances which could cause differences in the calibration and resulting soil moisture measurements between the seasons. The influence of the litter layer in forested environments was investigated by Bogena et al. (2013). Water content in the litter layer changes rapidly and adds unwanted temporal variability to the CRS time series. Therefore, Bogena et al. (2013) recommended considering the water dynamics in the litter layer explicitly in the calibration approach. Franz et al. (2013) introduced a new approach (the universal calibration function) that takes into account all sources of hydrogen thereby requiring estimates of lattice water, soil organic carbon, and vegetation biomass as well as a calibration factor retrieved from neutron count measurements over a large water body (500 m on all sides and deeper than 1 m).

Since the launch of the cosmic ray neutron method many changes and corrections have been brought forward that altered the way the method is applied. These changes and corrections can be divided into two groups. On the one hand, there are corrections that are applied to the raw neutron count in order to remove the influence that other variables have on the signal (such as air pressure and humidity variations or fluctuations in incoming neutron counts). On the other hand, changes have been made to the way we average the soil moisture measurements during the calibration campaigns in order to get a representative soil moisture value that corresponds to what the sensor actually "sees" at the time of calibration (changing critical depth, changing footprint, inclusion of lattice water and soil organic matter water equivalent). All this has

HESSD
12, 9813–9864, 2015

led to improvements in the method's accuracy for many environments. Most of these studies were performed in medium to high-count environments with count rates above 1000 counts per hour, in generally dry environments, at higher elevations and with little vegetation. Only a few studies were performed in low-count environments with count rates below 1000 counts per hour (e.g. Rivera Villareyes et al., 2011; Bogena et al., 2013). In the present study, we evaluated whether the CRS also provides reliable and consistent soil moisture measurements in a low-count environment, i.e., in a temperate mixed forest close to sea level. We tested several weighting approaches to convert gravimetrically determined soil water content of the top 30 cm into an average soil water content that can be used for the calibration of the CRS. Additionally, we analyzed whether the annual forest cycle of foliation and defoliation is important to consider for instrument calibration. Finally, we compiled a best-practice for the calibration of CRS in forested, low-count environments.

2 Field site and instrumentation

The CRS (CRS-1000 by Hydroinnova) was installed in the Müritz National Park in north-eastern Germany (53°19′49.0″ N, 13°11′56.5″ E) at an elevation of about 84 m a.m.s.l. (Fig. 1). Precipitation, temperature and relative humidity data was provided by the climate station Serrahn (1.6 km to the north). Average annual air temperature at the site is 8 °C with a maximum in July (17.2 °C) and a minimum in January (−0.9 °C). Average annual precipitation is 580 mm with a maximum in June (65 mm) and a minimum in February (28 mm). This makes for a maritime temperate climate (Cfb) in the Köppen climate classification. The sensor is located in a sandy outwash plain, a relic from the last glaciation, which causes the soil texture to be ~~relatively~~ homogeneous with sand fractions of about 95 % throughout the entire profile. Data from a nearby well shows that the groundwater level at the site is almost 20 m below the terrain surface. The vegetation within the sensor footprint consists of both deciduous and coniferous trees. Immediately surrounding the sensor is a mature beech forest

HESSD
12, 9813–9864, 2015

(*Fagus sylvatica* L., older than 100 years), also within the footprint (but farther away) with a distance of at least 40 m from the sensor there is young pine (*Pinus sylvestris* L.), oak (*Quercus robur* L.) and spruce (*Picea abies* (L.) H. Karst.) forest (all younger than 50 years) as well as a small strip of open grassland (see Fig. 2 and also Fig. 6 for a map of the forest stands within the footprint). Depending on the tree species, the mineral soil is covered by an organic soil layer and a litter layer of variable depth and water holding capacity.

For validation of the CRS soil water content measurements, we installed 18 soil moisture sensors (TOMST) close to the soil sampling/calibration locations. They are based on the principle of time domain transmission (TDT) and each sensor comes with its own logger and power supply (more information under: http://www.tomst.cz/tms/TMS-3.html). These sensors were installed vertically from the terrain surface into the soil so that they continuously measure soil water content averaged over the top 15 cm of the soil. In order to calibrate the sensors we used the gravimetric soil moisture data we collected from the upper 15 cm during the last five calibration campaigns (SU, F1–F4). The volumetric water content within the upper 15 cm of the CRS footprint was calculated as the mean of all 18 TDT sensors.

3 Methods

3.1 Calibration

We conducted a total of 10 calibration campaigns throughout one calendar year (2014). The first one (WI) took place in February during winterly conditions with very wet soils. The next four calibrations (S1–4) followed in spring (April–May) and covered the entire period of tree foliation. The sixth calibration (SU) was done under very dry conditions in July and the last four calibrations (F1–4) in fall (October-November) covering the trees' defoliation. For all the calibration campaigns we followed the recommended sampling pattern for the calibration of CRS which was detailed in Franz et al. (2012b). The

HESSD
12, 9813–9864, 2015

sampling pattern prescribes 3 concentric circles around the CRS with radii of 25, 75 and 200 m, respectively (Fig. 2). The 3 circles are intersected by 6 straight lines that point from the sensor towards north (0°), north-east (60°), south-east (120°), south (180°), south-west (240°) and north-west (300°). Samples are taken in the vicinity of all intersections – the samples do not have to be taken at the exact spot of the intersection. This sampling pattern ensures that each sample has equal weight towards the spatial mean of soil moisture that is detected by the CRS, assuming that the sensitivity of the CRS decreases exponentially with distance. We used a split-tube sampler to extract 30 cm soil cores at 18 locations within the footprint of the sensor afterwards dividing each soil core into six 5 cm thick soil samples. For each of the 10 calibrations this left us with 108 soil samples which were then transferred in sealed plastic bags to the laboratory where they were immediately weighed, then oven-dried at 105 °C for 24 h and then weighed again to determine their volumetric water content and bulk density. Afterwards, lattice water, soil organic matter content and root biomass were determined for six depth-representative soil samples. To this end the 108 samples (taken from the last calibration campaign in November) were grouped by sampling depth. We extracted 2 g of all 18 samples from one sampling depth and combined them to create one bulk sample per depth. Then, the already oven-dried samples were weighed and put in the oven for another 24 h at a temperature of 400 °C. This removed most of the soil organic matter and root biomass from the samples. After weighing the samples (to compute the fraction of combined soil organic matter and root biomass) they were again placed in the oven for 24 h, this time at a temperature of about 1000 °C. After that, the lattice water was also removed from the samples. A final weighing yielded the fraction of lattice water per soil depth. In order to make soil organic matter and root biomass comparable to the influence of pure water we converted them into equivalents of water by multiplying their weight by 0.556 which is the ratio of five times the molecular weight of water to the molecular weight of cellulose (taking into account that cellulose ($C_6H_{10}O_5$) contains 10 hydrogen atoms per molecule while water (H_2O) only contains two) (Hawdon et al., 2014).

HESSD
12, 9813–9864, 2015

The neutron counts from the sensor were smoothed with a 12 h moving window to reduce measurement noise (see Bogena et al., 2013). The next step was to correct the neutron counts for variations in (a) pressure, (b) incoming neutron flux and (c) water vapor in the air. This was done by applying the following corrections:

a. Pressure correction:

$$N_p = N_{raw} \cdot e^{\left(\frac{P-P_0}{L}\right)} \quad (1)$$

with N_p being the pressure corrected neutron counts ($n\,h^{-1}$), N_{raw} the raw neutron counts ($n\,h^{-1}$), P the atmospheric pressure (measured directly in the CRS case) for every time step (hPa), P_0 the average atmospheric pressure (hPa) for the entire measurement period and L the effective nucleon attenuation length for high-energy neutrons (for our site we assumed a value of 133.3 hPa) (Desilets and Zreda, 2003).

b. Incoming flux correction:

$$N_{pi} = N_p \cdot \frac{N_{avg}}{N_{nm}} \quad (2)$$

with N_{pi} being the sensor neutron count rate corrected for changes in atmospheric pressure and incoming neutrons ($n\,h^{-1}$), N_{avg} the average count rate of incoming neutrons ($n\,h^{-1}$) over the entire measurement period and N_{nm} the neutron count rate of the neutron monitor for each time step ($n\,h^{-1}$).

As the time series of the closest neutron monitor, located in Kiel, Germany, contains several data gaps, we selected the continuous time series of the Jungfraujoch, Switzerland, for this study. We scaled this time series by adjusting its mean ($309\,n\,h^{-1}$) to the mean of the Kiel time series ($327\,n\,h^{-1}$) in order to account for the difference in altitude and latitude between the two neutron

HESSD
12, 9813–9864, 2015

monitors. The resulting time series resembles the Kiel time series very closely (Fig. 3).

c. Water vapor correction:

$$N_{\mathrm{pih}} = N_{\mathrm{pi}} \cdot \left[1 + 0.0054 \cdot \left(p_{v0} - p_{v0}^{\mathrm{ref}}\right)\right] \tag{3}$$

with N_{pih} being the sensor neutron count corrected for changes in pressure, incoming neutrons and water vapor ($\mathrm{n\,h^{-1}}$), p_{v0}^{ref} the average absolute humidity of the air over the entire measurement period ($\mathrm{g\,m^{-3}}$) and p_{v0} the absolute humidity for each time step ($\mathrm{g\,m^{-3}}$). The constant 0.0054 has units of $\mathrm{m^3\,g^{-1}}$.

Finally, to convert corrected neutron counts (N_{pih}) into volumetric soil moisture (θ), Desilets et al. (2010) introduced an equation with four parameters – three of which (a_0 = 0.0808, a_1 = 0.372, a_2 = 0.115) were determined via neutron transport simulations and a fourth one (N_0) that serves as a calibration parameter accounting for site and sensor specific variations and representing neutron counts over dry soil at reference conditions during calibration:

$$\theta(t) = \left\{\left[a_0 \cdot \left(\frac{N_{\mathrm{pih}}(t)}{N_0} - a_1\right)^{-1} - a_2\right] \cdot \rho_{\mathrm{bd}}\right\} - W_{\mathrm{L}} - (\mathrm{SOM} + B_{\mathrm{R}}) \tag{4}$$

The other parameters ρ_{bd}, W_{L}, SOM and B_{R} can be measured directly from the calibration samples: the bulk density of the soil (ρ_{bd} in $\mathrm{g\,cm^{-3}}$), the summed volume fraction of lattice water in the soil grains and tightly bound water (W_{L} in $\mathrm{cm^3\,cm^{-3}}$), the combined volume fraction of soil organic matter and root biomass water equivalent (SOM + B_{R} in $\mathrm{cm^3\,cm^{-3}}$). In order to calibrate the sensor one first has to determine the depth- (and distance-) weighted averages for ρ_{bd}, W_{L}, SOM + B_{R} and θ as well as N_{pih} (averaged over 12 h) for the time of calibration. This is necessary because several

HESSD
12, 9813–9864, 2015

factors can influence the critical depth z^* (which is the depth of the soil layer up to which 86 % of the neutrons that the CRS detects originate from) and the footprint size of the sensor (Fig. 4). Afterwards N_0 is adjusted iteratively (e.g. with a simple Solver routine in Microsoft Excel) until the right-hand side of the equation equals the left-hand side.

We tested four soil moisture weighting approaches (Table 1), described in detail below, to determine which information is necessary for an accurate calibration. In a fifth approach we also tested whether including the influence of above-ground biomass (B_{ag}) further improves the performance of soil moisture retrieval with the CRS.

1. In the first approach (simple depth-weighting, SDW) a linear depth-weighting function was used (Franz et al., 2012b), where wt(z) represents the weight that is applied to the soil moisture measurements from a certain soil depth z:

$$\begin{cases} \mathrm{wt}(z) = a\left[1 - \left(\frac{z}{z^*}\right)^b\right] & 0 \le z \le z^* \\ \mathrm{wt}(z) = 0 & z > z^* \end{cases} \quad (5)$$

where

$$a = \frac{1}{z^* - \frac{z^* b+1}{(b+1)z^{*b}}} \quad (6)$$

and

$$z^* = \frac{5.8}{\frac{H_p}{\rho_w} + 0.0829} \quad (7)$$

and

$$H_p = W_L + \mathrm{SOM} + B_R + \rho_w\theta \quad (8)$$

In these equations z is the soil depth below the surface in cm and z^* is the critical soil depth in cm, a is a parameter that ensures that the weights are conserved, b

HESSD
12, 9813–9864, 2015

controls the curvature of the weighting function and is 1 for linear weighting, ρ_w is the density of water (here assumed to be 1 g cm^{-3}), H_p is the hydrogen content of belowground hydrogen pools (g cm^{-3}), W_L is lattice water (g cm^{-3}), SOM is soil organic matter water equivalent (g cm^{-3}), B_R is root biomass water equivalent (g cm^{-3}) and θ is the gravimetrically determined volumetric soil pore water content (m^3 m^{-3}). The original approach by Franz et al. (2012b) was modified by Bogena et al. (2013) using the total hydrogen content of belowground hydrogen pools H_p instead of just using the volumetric soil water content θ. Since H_p changes with soil depth we used an iterative approach to determine the appropriate weights. Starting with an average value for the upper 30 cm of the soil we computed a critical depth z^* and weighted H_p of the different soil depths accordingly. With this new value of H_p we then recomputed z^* and the weights. Usually the value of H_p stabilizes after a few iterations. The bulk density (ρ_{bd}) of the soil changes with depth and influences the soil moisture measurements too. Therefore it was also being taken into account during the iterative process of determining the critical depth z^* and the weighted soil moisture. In this weighting approach we did not use our depth-specific measurements of W_L and SOM + B_R, instead we assumed an average weight fraction value of combined W_L + SOM + B_R for the entire 30 cm profile.

2. The second approach (depth-specific weighting, DSW) was identical to the first one (SDW) except for using depth-specific measurements of W_L and SOM + B_R (see Table 2 for an example).

3. For the third approach (distance-depth-weighting, DDW) we adopted the weighting approach described in Köhli et al. (2015). This approach introduces distance-dependent variable depth-weighting where the critical depth decreases

HESSD
12, 9813–9864, 2015

with distance from the sensor. The critical depth z^* is calculated according to:

$$z^* = \rho_{bd}^{-1}\left[8.32 + 0.14 \cdot \left(0.97 + e^{\frac{-r}{100}}\right) \cdot \frac{26.42 + H_p}{0.057 + H_p}\right] \quad (9)$$

where ρ_{bd} is the bulk density of the soil ($g\,cm^{-3}$), r is the radial distance (in meters) from the CRS and H_p is the total hydrogen content of belowground hydrogen pools (see Eq. 8). This approach also assumes that the footprint size of the sensor varies with soil water content and atmospheric water content. We computed the varying footprint diameter for each calibration campaign and weighted the samples from 25, 75 and 200 m accordingly.

4. The fourth approach (distance-depth-weighting, non-linear, DDWnl) was identical to the third one (DDW) except for using the non-linear depth-weighting function recommend by Köhli et al. (2015) instead of the linear one (from Eq. 5):

$$wt(z) = e^{\frac{-2z}{z^*}} \quad (10)$$

5. In the fifth approach, an above-ground biomass correction (ABC) was added to the third approach (DDW). This approach differs from the first four weighting approaches by explicitly correcting the neutron counts for vegetation effects, i.e., it corrects neutron counts for the additional damping by above-ground biomass without altering the depth weighting of the calibration function itself. To this end, we adopted the method proposed by Baatz et al. (2015) to further correct the neutron signal already corrected for pressure, incoming flux and water vapor (N_{pih}) and derive a vegetation-corrected neutron count (N_{pihv}). According to Baatz et al. (2015) vegetation causes a neutron intensity reduction by 0.9 % per kg of dry aboveground biomass (B_{ag}) per m^2:

$$N_{pihv} = \frac{N_{pih}}{1 - \left(0.009 \cdot B_{ag}\right)} \quad (11)$$

HESSD
12, 9813–9864, 2015

At our field site this means an intensity reduction of 57.3 % due to the beech forest surrounding the CRS (B_{ag} = 63.8 kg m^{-2}, see Sect. 3.2). The seasonal variation due to the presence of leaves on the trees is negligible (winter: B_{ag} = 62.8 kg m^{-2}; intensity reduction = 56.5 %), not even considering the fact that the leaves are still present as litter on the ground.

3.2 Estimation of biomass and influence of seasonal changes in biomass

Biomass influences neutron counts due to its hydrogen content. In order to test (and potentially exclude) the influence of seasonal changes in aboveground forest biomass, a survey of the beech tree stand around the CRS was conducted. We estimated living tree biomass and tree biomass changes throughout the year by applying the aboveground dry biomass functions for beech forest (*Fagus sylvatica* L.) from Santa Regina et al. (1997):

$$B_S = 0.0894 \cdot \mathrm{DBH}^{2.4679} \quad (12)$$

$$B_B = 0.0317 \cdot \mathrm{DBH}^{2.3931} \quad (13)$$

$$B_L = 0.0145 \cdot \mathrm{DBH}^{1.9531} \quad (14)$$

B_S is dry stem biomass (kg tree^{-1}), B_B dry branch biomass (kg tree^{-1}), B_L dry leaf biomass (kg tree^{-1}) and DBH is the diameter of the tree stem at breast height (cm).

To apply these functions we conducted a survey of tree diameters and tree density in the beech forest that surrounds the CRS. This allowed us to determine both the total biomass of the beech forest, as well as the seasonally variable fraction of biomass (leaf biomass divided by total biomass). The seasonally variable fraction of hydrogen mass in the trees aboveground can introduce a second temporally dynamic signal on neutron counts. In order to determine this fraction we first calculated the water mass in stems, branches and leaves (assuming a leaf water content of 0.6 kg kg^{-1} (Gravano

HESSD
12, 9813–9864, 2015

et al., 1999) and a wood water content of 0.11 $kg\,kg^{-1}$ (Bouriaud et al., 2004)) and then converted the water and dry biomass values into hydrogen equivalents by assuming that the weight fraction of hydrogen in water is 0.1198 $kg\,kg^{-1}$ (H_2O) and the hydrogen content in biomass is 0.0622 $kg\,kg^{-1}$ (Cellulose: $C_6H_{10}O_5$).

The tree survey revealed a median diameter of 23.9 cm (Min: 3.2 cm, Q_{25}: 11.5 cm, Q_{75}: 43.7 cm, Max: 93.3 cm) and a tree density of 0.05 trees m^{-2}. With these values at hand and Eqs. (12)–(14) the dry above-ground biomass of the beech stand (B_{ag}) was computed to be 63.8 $kg\,m^{-2}$ (with 62.8 $kg\,m^{-2}$ from stem and branches and 1.0 $kg\,m^{-2}$ from leaves) (Fig. 5). Assuming a water content of 0.11 $kg\,kg^{-1}$ for wood and a water content of 0.6 $kg\,kg^{-1}$ for leaves results in 9.2 $kg\,m^{-2}$ of biomass water (W_{agb}) (with 7.8 $kg\,m^{-2}$ from stem and branches and 1.5 $kg\,m^{-2}$ from leaves). Finally, using the mass fraction of hydrogen in water (M_w = 0.1119 $kg\,kg^{-1}$) and in dry biomass (M_b = 0.0622 $kg\,kg^{-1}$) one can calculate the total hydrogen density (H_{agb}) of above-ground biomass in the beech stand:

$$H_{agb} = W_{agb} \cdot M_w + B_{ag} \cdot M_b \quad (15)$$

Our calculations yielded a hydrogen density of 4.8 $kg\,m^{-2}$ for stem and branches and a hydrogen density of 0.2 $kg\,m^{-2}$ for leaves. Assuming that the hydrogen content of the stem and branches is constant and only the leaves change seasonally one is left with a fraction of variable hydrogen in the above-ground biomass that accounts for 7.7 % of the total hydrogen mass. At high soil moisture, a 0.01 $m^3\,m^{-3}$ soil moisture change from 0.19 to 0.20 $m^3\,m^{-3}$ equals a change of 0.07 $kg\,m^{-2}$ of hydrogen in the soil. At low soil moisture the change from 0.05 to 0.06 $m^3\,m^{-3}$ is equal to a change in hydrogen of 0.25 $kg\,m^{-2}$ (due to the fact that the CRS also receives the neutron signal from deeper soil depths (larger critical depth z^*)).

HESSD
12, 9813–9864, 2015

3.3 Validation

As an objective performance measure to compare the soil moisture time series derived from the CRS with the soil moisture time series from the TDT sensors we used the modified Kling–Gupta efficiency KGE' (Gupta et al., 2009; Kling et al., 2012):

$$\mathrm{KGE}' = 1 - \sqrt{(r-1)^2 + (\beta-1)^2 + (\gamma-1)^2} \quad (16)$$

With correlation coefficient r, bias ratio $\beta = \mu_{\mathrm{mod}}/\mu_{\mathrm{obs}}$ and variability ratio $\gamma = (\sigma_{\mathrm{mod}}/\mu_{\mathrm{mod}})/(\sigma_{\mathrm{obs}}/\mu_{\mathrm{obs}})$.

4 Results

4.1 Gravimetric soil water measurements and soil physical characteristics

The spatial distribution of volumetric soil water content for the 10 calibration days is shown in Fig. 6. At each location the soil water content is an unweighted average value of the six samples taken from 0 to 30 cm depth. The mean volumetric soil water content for the calibration days over all calibration locations ranged from 0.07 up to 0.16 $\mathrm{m^3\,m^{-3}}$ with standard deviations ranging from 0.015 to 0.047 $\mathrm{m^3\,m^{-3}}$. A general soil moisture pattern emerged with the soil moisture under coniferous tree stands being lower and under deciduous tree stands being higher. Especially the uppermost soil layer (0–5 cm) was drier under the coniferous trees – on average about 0.065 $\mathrm{m^3\,m^{-3}}$ – while the deeper soil layers under coniferous trees were about 0.023 $\mathrm{m^3\,m^{-3}}$ drier. The highest spatial variabilities in soil moisture were encountered during spring and fall seasons and more homogenous soil moisture conditions during winter and summer.

The average bulk density (ρ_{bd}) measurements for the 10 calibration campaigns ranged from 1.16 to 1.22 $\mathrm{g\,cm^{-3}}$ (mean: 1.18 $\mathrm{g\,cm^{-3}}$, standard deviation: 0.02 $\mathrm{g\,cm^{-3}}$). The weight fraction of soil organic matter and root biomass water equivalent (SOM+B_{R})

HESSD
12, 9813–9864, 2015

was determined to be 51.4 g kg^{-1} in the shallowest soil layer (0–5 cm) with decreasing values at depth. The weight fraction of lattice water (W_L) was determined to be 3.2 g kg^{-1} in the shallowest soil layer with slightly increasing values at deeper soil depths.

4.2 Calibration

The average reference atmospheric pressure (P_0) for the entire measurement period was 1005.8 hPa; the average reference incoming neutron flux (N_{avg}) was 328.3 n h^{-1}; the average reference absolute humidity (p_{v0}^{ref}) was 9.1 g m^{-3}. Equations (5) through (10) were used to calculate the depth-weighted volumetric soil water content (θ_{depthW} and $(H_p)_{depthW}$) according to the four weighting approaches we applied. Equations (1)–(3) were used to compute N_p, N_{pi} and N_{pih} (as well as Eq. 11 to compute N_{pihv}), and then Eq. (4) to identify N_0 for each calibration. Table 2 provides an example of the depth-weighting following approach 2 (DSW with depth-specific values of W_L and SOM + B_R).

The values in Table 2 result in a depth-weighted average volumetric water content θ_{depthW} of 0.150 cm^3 cm^{-3}, a depth-weighted volumetric water content including W_L and SOM + B_R $(H_p)_{depthW}$ of 0.179 cm^3 cm^{-3} and a depth-weighted bulk density $(\rho_{bd})_{depthW}$ of 0.981 g cm^{-3}. If W_L and SOM + B_R were not considered, the values for θ_{depthW} and $(\rho_{bd})_{depthW}$ would change to 0.146 cm^3 cm^{-3} and 1.013 g cm^{-3} respectively, because the critical depth z^* increases when the higher amounts of SOM + B_R in the shallow layers are not considered, thus giving more weight to low soil moisture values in deeper soil horizons.

4.3 Footprint variability

The footprint diameters calculated according to Köhli et al. (2015) and used in approaches 3–5 ranged from 185 to 200 m. This resulted in distance weights of ~ 0.56

HESSD
12, 9813–9864, 2015

(for samples from 25 m), ∼ 0.35 (for samples from 75 m) and ∼ 0.10 (for samples from 200 m). These weighting factors varied only marginally between the individual calibration campaigns.

Table 3 lists the parameters relevant for calibration for all 10 calibration dates (again following approach 2, SDW, with depth-specific values of W_L and SOM + B_R).

Ideally, we would have ended up with 10 identical N_0 calibration parameters. However, the range we found was considerable – from 858 to 910 $n\,h^{-1}$ (mean: 878 $n\,h^{-1}$, standard deviation: 13.8 $n\,h^{-1}$). As a consequence, the 10 computed time series based on the standard N_0-calibration function of Desilets et al. (2010) showed differences of more than 0.1 $m^3\,m^{-3}$ in volumetric soil water content, especially during conditions of high soil moisture (Fig. 7).

In fact, none of the five approaches was able to solve this problem. All resulted in largely deviating N_0-values and time series of volumetric soil water content between the individual calibrations (Table 4).

4.4 New calibration function

To include all information of our 10 calibration campaigns into our analysis, we fitted new calibration functions to our five sets of 10 calibration points each. This was done by using the Microsoft Excel Solver software to optimize the three shape parameters (a_0, a_1, a_2) and N_0 through the calibration point cloud (solid lines in Fig. 8). Plotting the N_{pih}-values of all 10 calibrations against the gravimetrically determined and depth- (and distance-) weighted volumetric soil moisture revealed that the standard shape of the soil moisture-neutron count relation is not valid at our field site. Instead of plotting along functions defined by the standard calibration (Desilets et al., 2010) (examples are dotted lines in Fig. 8) our calibration points are better captured by less steep functions (solid lines in Fig. 8 are the best-fit calibration functions for the different approaches). Using the N_0-calibration function with the standard shape parameters may lead to large soil water content deviations between individual

HESSD
12, 9813–9864, 2015

calibration campaigns, especially under wet soil moisture conditions. The slope of the N_0-calibration function is essentially too steep, which means that in our environment a change in the neutron count is caused by a more subtle change in soil moisture than is assumed by the standard relationship – essentially the sensor is more sensitive than expected.

The optimized parameters for the five approaches are shown in Table 5. The resulting soil moisture time series are shown in Fig. 9.

4.5 Validation

We tested whether the new calibration functions improved the performance of the CRS measurements relative to in situ measurements, and if so, which of the approaches performed best. In order to do that we compared the soil moisture time series from the CRS (using the standard N_0-calibration function from Desilets et al. (2010) and applying our newly derived corrected relationships) with the soil moisture time series from the TDT sensors distributed throughout the footprint. As a first step, the CRS measurements had to be converted to a soil water content value representative of the top 15 cm of the soil (the integration depth of the TDT sensors). For this purpose we compared the weighted volumetric water content (θ_{depthW}) from the gravimetric measurements of the calibration campaigns (basically what the CRS is supposed to "see") with the unweighted average gravimetric measurements of the top 15 cm ($\theta_{15\,\mathrm{cm}}$). We found strong linear correlations for two of the weighting approaches (SDW and DSW) with CRS water content being larger than the $\theta_{15\,\mathrm{cm}}$ values and increasing differences for wetter soil conditions (indicating that for higher soil moisture the CRS overestimates soil water contents in the top 15 cm while for lower soil moisture the overestimation decreases). For approaches 3–5 (DDW, DDWnl and ABC) an offset of 0.005 $\mathrm{m^3\,m^{-3}}$ indicated slightly lower CRS soil water content than the top 15 cm values. We then converted the CRS time series by the above relationships into time series that were representative of the top 15 cm and compared them to the TDT measurements. The modified Kling–Gupta efficiency

HESSD
12, 9813–9864, 2015

(KGE') was used as a performance measure. The worst performance was achieved by the simple depth weighting approach (KGE'(SDW) = 0.83, Table 6), the performance improved when depth-specific weighting was included (KGE'(DSW) = 0.88) and it further improved when including distance weighting (KGE'(DDW) = 0.92). The linear depth weighting worked better than the non-linear depth weighting (KGE'(DDWnl) = 0.87). The inclusion of a vegetation correction did not improve the performance any further (KGE'(ABC) = 0.92). That means that the distance–depth-weighting approach (DDW) improved the neutron sensors performance the most. In comparison, using the single-point standard N_0-calibration function and DDW yielded KGE's for the individual calibration campaigns ranging from 0.46 to 0.79 with a mean KGE' of 0.68 (±0.09). It is important to note that all of the new calibration approaches performed better than their standard calibration counterparts. The improvement of performance of the new N_0-calibration functions compared to the standard calibration functions was caused by the better agreement of both the bias ratios β and the variability ratios γ, i.e. both the means and the variabilities of the CRS time series better matched the TDT observations (see also Fig. 10). This supports the hypothesis that at our field site changes in neutron count are caused by more subtle changes in soil moisture than expected.

4.6 Optimizing calibration efforts

We further tested whether two or more individual calibration campaigns are required to determine a comprehensive calibration function shape, and under which soil moisture conditions these calibrations should be conducted. We paired each individual calibration point (derived from the best-performing weighting approach, DDW) with all the other calibration points (WI and S1, WI and S2, WI and S3, etc.) and computed best-fit calibration functions for all of these pairings (Fig. 11).

Then we used the resulting calibration functions to convert the measured neutron counts into time series of volumetric soil water content and compared these to the TDT measurements (again using the KGE' as the performance measure). We found that

HESSD
12, 9813–9864, 2015

a two-point calibration proved to be sufficient in case that the difference in soil water content between the two calibrations was at least 0.12 $m^3 m^{-3}$ (i.e. for our sandy soils it covered 50 % of the observed range of soil water content). Also, it turned out to be more important to capture a calibration point at very dry rather than at very wet soil water contents. This is illustrated in Fig. 12 where predominantly calibrations that involve low soil water contents (red dots) as the minimum value achieve KGE's of 0.9 while these KGE' values are also achieved more frequently with intermediate soil water contents (light blue dots) as the maximum value.

4.7 Other potential influences on neutron count

In search of potentially unaccounted factors that influence the neutron count we compared N_0-values obtained from the 10 calibrations with apparent atmospheric pressure, specific humidity, temperature and estimates of forest crown cover (derived from photographs taken from the ground aiming at the zenith) during the calibration campaigns. No seasonal or other temporal relationships were found.

Assuming a linear depth-weighting function, the total amount of hydrogen from pore water that a CRS "sees" is 4.01 $kg m^{-2}$ for a soil water content of 0.20 $m^3 m^{-3}$ (critical depth = 17.9 cm) while it reduces to 3.93 $kg m^{-2}$ for a soil water content of 0.19 $m^3 m^{-3}$ (critical depth = 18.5 cm). That means that a change in volumetric soil water content of 0.01 $m^3 m^{-3}$ is equal to a change in hydrogen of 0.08 $kg m^{-2}$. However, the same change in soil water content under drier conditions is associated with a larger change in hydrogen: if the soil water content is 0.06 $m^3 m^{-3}$ (critical depth = 31.6 cm), the CRS "sees" 2.12 $kg m^{-2}$ of hydrogen, if the soil water content is 0.05 $m^3 m^{-3}$ (critical depth = 33.4 cm) then the CRS "sees" only 1.87 $kg m^{-2}$ – so the difference in hydrogen is 0.25 $kg m^{-2}$. The variability in hydrogen due to foliation and defoliation in the beech forest surrounding the CRS amounts to 0.22 $kg m^{-2}$. This means that it equals a change in soil water content of about 0.031 $m^3 m^{-3}$ (under wet conditions) and 0.009 $m^3 m^{-3}$ (under dry conditions). These differences for wet and dry conditions are due to the fact that the critical depth of the sensor is larger during dry conditions

HESSD
12, 9813–9864, 2015

and therefore an equal increase in soil water content requires a larger amount of water since a larger soil column has to be filled. These calculations disregard the fact that fallen leaves still contain hydrogen (which hence is not completely removed from the system immediately and therefore should also reduce the expected variability). At our field site 65 % of the distance-weighted area surrounding the CRS is covered by deciduous trees (mainly beech and oak), the other 35 % do not experience a significant annual cycle of leaf growth and fall (pine, spruce and grassland). This should further reduce the influence of seasonally variable biomass on the cosmic ray neutron counts (with a potential maximum influence of leaf-out during wet conditions of 0.020 $m^3 m^{-3}$ and only 0.006 $m^3 m^{-3}$ in dry conditions). In summary, we do not expect a significant impact of seasonally varying above-ground biomass on the measurements of soil water content.

5 Discussion

The tenfold standard calibration of our CRS produced 10 different time series of volumetric water content. The differences between the individual time series at times exceeded 0.1 $m^3 m^{-3}$. Moreover, the time series of soil water content derived from the neutron counts via the standard N_0-calibration function exhibited a variability that was too high compared to the distributed continuous in situ measurements. Altering the shape of the calibration function led to much higher congruence between the individual calibration efforts. Furthermore, the determination of a new calibration function enhanced the performance of the CRS measurements significantly when comparing them with independent distributed measurements of soil water content. Different weighting approaches proved to be more or less useful in identifying appropriate soil water contents for the time of calibration campaigns. The fact that the depth-specific weighting (DSW) approach performed better than the simple depth weighting (SDW) is an indication that the depth variations in lattice water, soil organic matter and root biomass content should be explicitly represented during the calibration

HESSD
12, 9813–9864, 2015

of the CRS. The best performance was achieved with a weighting approach that explicitly takes into account both depth-weighting as well as distance weighting of the soil water content. This suggests that the variation in the footprint diameter needs to be considered during individual calibration campaigns. Linear depth-weighting resulted in a better CRS performance than non-linear depth-weighting since the non-linear depth-weighting basically underestimated soil water contents during wet periods (because higher weights of deeper (drier) soil layers were included). This caused both a decrease in the mean soil water content as well as a decrease in the variability of the soil water content time series and hence reduced the performance of the CRS. Adding a correction for above-ground biomass to the time series of neutron counts (converting N_{pih} to N_{pihv} using Eq. 11) did not improve the performance of the CRS measurements. It only marginally changed the shape of the calibration function and produced almost the same time series of soil water content as the version without any correction for above-ground biomass. Also, we could not find systematic changes in the calibration results connected to the annual cycle of tree foliation/defoliation (i.e. a reduction in counts during summer due to higher hydrogen content in the above-ground biomass). Furthermore, our calculations of variable hydrogen mass in the canopy suggested that these seasonal changes are small compared to the changes of hydrogen mass in the soils caused by changes in soil water content. Therefore we deem a correction for variable forest canopy hydrogen at different times of the year unnecessary.

The differences in calibration results are more likely caused by the fact that the shape of the N_0-calibration function is different at our field site. That means that while being temporally stable the shape of the calibration function is spatially variable – there is no standard curve applicable to all sites. At our site the function is less steep than the standard N_0-calibration function suggested by Desilets et al. (2010), i.e. a similar increase in neutron counts is associated with a smaller decrease in soil moisture. A recalibration of the shape of the curve using all calibration points considerably improved the agreement between in situ measurements and CRS measurements of soil moisture. A two-point calibration already proved to be sufficient to define the correct

HESSD
12, 9813–9864, 2015

shape of the calibration function given that the soil moisture states at the two calibration times are sufficiently different.

We can only speculate about the reasons behind this shape inconsistency of the calibration function since we did not do any theoretical neutron modeling. To our knowledge at our site we are dealing with the lowest number of counts of all published studies (average $N_0 = 878\,\mathrm{n\,h^{-1}}$, Table 3). Although the calibration function was theoretically developed for all environments it has probably never been tested sufficiently in such low-count, forested environments. And while the shape of the function seems to work well in high-count environments, it clearly does not at our site. Bogena et al. (2013) pointed out another complicating factor that is present in forested environments – the litter layer. They showed that at their sites (N_0: 913 to $1397\,\mathrm{n\,h^{-1}}$) the water content within the litter layer was subject to much higher variability than the water content in the underlying soil. During wet conditions the litter layer contained 36 % of the hydrogen mass within the footprint of the CRS while during dry conditions it contained only 10 % of the hydrogen mass. This leads to an increase in the variability of the neutron counts and can thus cause an overestimation of soil water content during wet conditions. The occurrence of canopy interception would have the same variability-increasing effect on the CRS signal, although it is expected to be significantly smaller than the influence of the litter layer. We argue that an adjustment to the shape of the calibration function is able to solve this problem. By decreasing the slope of the calibration function we effectively reduce the sensitivity of the CRS and hence the temporal variability in the output signal (the time series of soil water content). Baatz et al. (2014) working also in a low-count environment (N_0: 936 to $1242\,\mathrm{n\,h^{-1}}$) with land use ranging from grassland to agriculture to forest compared the standard N_0-calibration method to another calibration method developed by Shuttleworth et al. (2013) (the COSMIC operator) and found that the former interpreted dry periods drier and wet periods wetter – which is also in accordance to our findings that suggest that the standard N_0-calibration function is too steep. Lv et al. (2014), in a study at a mixed-forest/grassland site also recommended more than

HESSD
12, 9813–9864, 2015

one calibration. They operated in a high-count environment in Utah ($N_0 = 2189\,\mathrm{n\,h^{-1}}$) and attributed the different shape of their calibration function to binary soil moisture patterns at their site where the grassland soils were much drier than the forest soils under wet conditions but just as dry under dry conditions. Our field site is subject to similar spatial variability since it is also comprised of multiple areas with non-uniform soil water content (mean values of soil water contents differ between different forest stands). The fact that distance weighting improved our results can be regarded as an indication that non-homogeneous soil moisture conditions also lead to changes in the shape of the calibration function. In a recent study Iwema et al. (2015) investigated temporal field sampling strategies for three different calibration methods. They also recommend more than one calibration campaign for the N_0-calibration approach and argue that the shape of the calibration function should not be fixed but variable during the calibration process.

If it was possible to fully correct for all factors that influence footprint size, depth-weighting and neutron count, a one-time calibration of the CRS would be sufficient. However, we think that when intending to use the CRS as a simple tool to measure soil water content at intermediate scales, the benefit of obtaining all corrections does not justify the effort required to measure all parameters necessary. Therefore we recommend a two-time calibration that – although being empirical in nature – inherently incorporates many of the required corrections.

6 Conclusion

Our results suggest that a one-time calibration of the CRS using the available neutron count corrections and weighting approaches is not sufficient at our field site. This is mainly due to the fact that the shape of the standard N_0-calibration function is not able to capture the dynamics in soil water content we observed with our network of distributed in situ TDT sensors. Several factors could cause this discrepancy, amongst them the presence of litter layers and spatially heterogeneous soil moisture conditions

HESSD
12, 9813–9864, 2015

within the sensor footprint. After calibrating the CRS 10 times in a mixed forest in north eastern Germany we found that a two-point calibration already considerably improves the agreement between soil water content derived from in situ TDT measurements and from the CRS, given significantly different moisture conditions during the two calibration periods/campaigns (for a detailed explanation on the procedure see Appendix A). We found that the explicit consideration of depth-specific values of soil organic matter and root biomass improved the calibration results while taking into account seasonal changes in above-ground biomass in the forest was unnecessary. While there is no doubt that further investigations on factors that influence the neutron signal are necessary and useful, it is also apparent that it becomes increasingly difficult to distinguish between the effects of the individual correction factors and the uncertainty caused by all the corrections. Therefore our goal was to use empirical data to test available methods and combinations thereof and to provide a guideline on how to easily and comprehensively calibrate a CRS in various environments using these methods. Looking beyond that objective, investigations in the form of site intercomparison studies along gradients from high to low-count environments and/or from locations with varying litter layers could give rise to the development of simple corrections to the shape of the N_0-calibration function.

When measuring soil water content with a CRS it is important to note that over time the measurements are hardly ever representative of the exact same soil segment around and below one sensor. With the footprint shrinking and expanding and the critical depth of the soil decreasing and increasing we have to be careful when interpreting and using our results. If we keep that in mind, however, this new technology will indeed be able to bridge the gap between point in-situ and areal remote sensing soil moisture measurements and thus provide a valuable tool for the advancement of hydrologic understanding.

HESSD
12, 9813–9864, 2015

Appendix A: Best practice for calibration in low-count forest environments

1. Set up (or use) a weather station that monitors air temperature and relative humidity close to the CRS.
2. Set up the CRS.
3. Switch on the CRS and come back later for calibration (or set it up before 6 a.m. and start calibrating on the same day). Do not switch it off after the calibration, let it record continuously.
4. Choose a day with very dry or very wet soil moisture conditions for the first calibration campaign and wait for the opposite conditions for your second calibration (this might take a full year to achieve, but you will not lose any data, you will just not be able to use the data immediately).
5. Choose days without rain or snow for your calibrations, litter and canopy should be dry.
6. Take 108 soil samples from 18 locations and six depths according to Franz et al. (2012b).
7. Weigh the samples the same day you take them, let them oven-dry for 24 h at 105 °C and weigh them again to determine the volumetric water content (θ) and the bulk density (ρ_{bd}).
8. Create six bulk samples from the six different soil depths (2 g from each of the 18 locations suffices for each soil depth).
9. Analyze the combined soil organic matter (SOM) and root biomass (B_R) content of the six bulk samples by weighing them (after regular oven-drying at 105 °C) and then heating them to a temperature of 400 °C for 24 h before weighing them again. Convert SOM and B_R to water equivalents by multiplying their weight by 0.556.

HESSD
12, 9813–9864, 2015

10. Analyze the lattice water (W_L) content of the six bulk samples by weighing them (after SOM and B_R extraction at 400 °C) and then heating them to a temperature of 1000 °C for 24 h before weighing them again.

11. Determine the average hydrogen content of belowground hydrogen pools (H_p) for each soil depth.
Equation (8).

12. Apply a linear weighting function to your gravimetrically determined H_p measurements accounting for the change in the critical depth z^* of the sensor and retrieve a weighted average of H_p within the footprint of the CRS by iteration. Start out by computing the critical depth z^* corresponding to your gravimetrically determined values of H_p and ρ_{bd} averaged over the entire 30 cm. Then apply the weights for the different soil depths z and update the values. Recalculate the critical depth z^* and continue this procedure until all values stabilize. Do this for each sampling/calibration distance (25, 75 and 200 m) separately.
Equations (5), (6) and (9).

13. Apply an additional distance-weight to the depth-weighted volumetric water contents from the different locations in order to account for variations in the footprint size. Also do this iteratively adjusting H_p and the distance weights until both become stable.
Equations are conveniently provided as a supplement by Köhli et al. (2015) in the form of an Excel sheet.

14. Use the depth-and-distance weights to compute weighted values of soil water content (θ), bulk density (ρ_{bd}), lattice water (W_L), soil organic matter and root biomass water equivalent (SOM + B_R).

15. Average raw neutron counts (N_{raw}) from the moderated sensor (measuring fast neutrons) over 12 h with a moving window.

HESSD
12, 9813–9864, 2015

16. Retrieve data from the neutron monitor close to your location in order to correct for the varying intensity of incoming neutrons (you may have to correct this data and fill gaps).

17. Using the entire time series for the period where cosmic-ray data is available determine average atmospheric pressure (P_0), average incoming neutron intensity (N_{avg}) and average absolute humidity (p_{v0}^{ref}).

18. Correct raw neutron counts for atmospheric pressure variations (N_p).
Equation (1).

19. Correct raw neutron counts for incoming neutron intensity variations (N_{pi}).
Equation (2).

20. Correct raw neutron counts for absolute humidity variations (N_{pih}).
Equation (3).

21. Plot the N_{pih} of both calibrations against the gravimetrically measured, distance- and depth-weighted volumetric soil water content (θ) according to the standard N_0-calibration function with fitting parameters.
Equation (4).

22. Fit a function through the two calibration points altering N_0, a_0, a_1 and a_2 (e.g. using Microsoft Excel solver). When doing this, use average values of the two calibration campaigns for bulk density (ρ_{bd}), lattice water (W_L), soil organic matter and root biomass water equivalent (SOM + B_R).

23. Use best fit parameters to convert time series of N_{pih} to volumetric soil water content.

Acknowledgement. Funding was provided by the Terrestrial Environmental Observatories (TERENO) and the Virtual Institute for Integrated Climate and Landscape Evolution (ICLEA). We would like to thank the Müritz National Park for allowing us to site our research in their

HESSD
12, 9813–9864, 2015

forest. Marvin Reich, Iris Heine, Lisei Köhn, Janek Dreibrodt, Stephan Schröder, Erik Reinholz, Christian Rippich, Christopher Gravesen all helped out in the field while Philip Müller and Hans-Peter Nabein assisted in the lab. Gabriele Baroni, Lena Scheiffele and Katja Mroos lent us their field equipment and Martin Schrön provided us with scripts for depth-distance-weighting.

The article processing charges for this open-access publication were covered by a Research Centre of the Helmholtz Association.

References

Baatz, R., Bogena, H. R., Hendricks Franssen, H.-J., Huisman, J., Qu, W., Montzka, C., and Vereecken, H.: Calibration of a catchment scale cosmic-ray probe network: A comparison of three parameterization methods, J. Hydrol., 516, 231–244, doi:10.1016/j.jhydrol.2014.02.026, 2014.

Baatz, R., Bogena, H. R., Hendricks Franssen, H.-J., Huisman, J. A., Montzka, C., and Vereecken, H.: An empirical vegetation correction for soil water content quantification using cosmic ray probes, Water Resour. Res., 51, 2030–2046, doi:10.1002/2014WR016443, 2015.

Bachelet, F., Balata, P., Dyring, E., and Iucci, N.: Attenuation coefficients of the cosmic-ray nucleonic component in the lower atmosphere, Il Nuovo Cimento, 35, 23–35, doi:10.1007/BF02734822, 1965.

Baroni, G. and Oswald, S.: A scaling approach for the assessment of biomass changes and rainfall interception using cosmic-ray neutron sensing, J. Hydrol., 525, 264–276, doi:10.1016/j.jhydrol.2015.03.053, 2015.

Bogena, H. R., Huisman, J. A., Baatz, R., Hendricks Franssen, H.-J., and Vereecken, H.: Accuracy of the cosmic-ray soil water content probe in humid forest ecosystems: the worst case scenario, Water Resour. Res., 49, 5778–5791, doi:10.1002/wrcr.20463, 2013.

Bouriaud, O., Bréda, N., Moguédec, G., and Nepveu, G.: Modelling variability of wood density in beech as affected by ring age, radial growth and climate, Trees, 18, 264–276, doi:10.1007/s00468-003-0303-x, 2004.

HESSD
12, 9813–9864, 2015

Coopersmith, E., Cosh, M., and Daughtry, C.: Field-scale moisture estimates using COSMOS sensors: a validation study with temporary networks and Leaf-Area-Indices, J. Hydrol., 519, 637–643, doi:10.1016/j.jhydrol.2014.07.060, 2014.

Desilets, D. and Zreda, M.: Spatial and temporal distribution of secondary cosmic-ray nucleon intensities and applications to in situ cosmogenic dating, Earth Planet. Sc. Lett., 206, 21–42, doi:10.1016/S0012-821X(02)01088-9, 2003.

Desilets, D. and Zreda, M.: Footprint diameter for a cosmic-ray soil moisture probe: theory and Monte Carlo simulations, Water Resour. Res., 49, 3566–3575, doi:10.1002/wrcr.20187, 2013.

Desilets, D., Zreda, M., and Ferré, T.: Nature's neutron probe: Land surface hydrology at an elusive scale with cosmic rays, Water Resour. Res., 46, W11505, doi:10.1029/2009WR008726, 2010.

Franz, T., Zreda, M., Ferre, T., Rosolem, R., Zweck, C., Stillman, S., Zeng, X., and Shuttleworth, W.: Measurement depth of the cosmic ray soil moisture probe affected by hydrogen from various sources, Water Resour. Res., 48, W08515, doi:10.1029/2012WR011871, 2012a.

Franz, T., Zreda, M., Rosolem, R., and Ferre, T.: Field validation of a cosmic-ray neutron sensor using a distributed sensor network, Vadose Zone J., 11, doi:10.2136/vzj2012.0046, 2012b.

Franz, T., Zreda, M., Rosolem, R., and Ferre, T.: A universal calibration function for determination of soil moisture with cosmic-ray neutrons, Hydrol. Earth Syst. Sc., 17, 453–460, doi:10.5194/hess-17-453-2013, 2013.

Gravano, E., Bussotti, F., Grossoni, P., and Tani, C.: Morpho-anatomical and functional modifications in beech leaves on the top ridge of the Apennines (Central Italy), Phyton Horn, 39, 41–46, 1999.

Gupta, H., Kling, H., Yilmaz, K., and Martinez, G.: Decomposition of the mean squared error and NSE performance criteria: Implications for improving hydrological modelling, J. Hydrol., 377, 80–91, doi:10.1016/j.jhydrol.2009.08.003, 2009.

Hawdon, A., McJannet, D., and Wallace, J.: Calibration and correction procedures for cosmic-ray neutron soil moisture probes located across Australia, Water Resour. Res., 50, 5029–5043, doi:10.1002/2013WR015138, 2014.

Hendrick, L. D. and Edge, R. D.: Cosmic-ray neutrons near the Earth, Phys. Rev., 145, 1023–1025, 1966.

HESSD
12, 9813–9864, 2015

Iwema, J., Rosolem, R., Baatz, R., Wagener, T., and Bogena, H. R.: Investigating temporal field sampling strategies for site-specific calibration of three soil moisture–neutron intensity parameterisation methods, Hydrol. Earth Syst. Sci., 19, 3203–3216, doi:10.5194/hess-19-3203-2015, 2015.

Kling, H., Fuchs, M., and Paulin, M.: Runoff conditions in the upper Danube basin under an ensemble of climate change scenarios, J. Hydrol., 424–425, 264–277, doi:10.1016/j.jhydrol.2012.01.011, 2012.

Kodama, M., Kudo, S., and Kosuge, T.: Application of atmospheric neutrons to soil moisture measurement, Soil Sci., 140, 237–242, 1985.

Köhli, M., Schrön, M., Zreda, M., Schmidt, U., Dietrich, P., and Zacharias, S.: Footprint characteristics revised for field-scale soil moisture monitoring with cosmic-ray neutrons, Water Resour. Res., 51, 5772–5790, doi:10.1002/2015WR017169, 2015.

Lv, L., Franz, T., Robinson, D., and Jones, S.: Measured and modeled soil moisture compared with cosmic-ray neutron probe estimates in a mixed forest, Vadose Zone J., 13, doi:10.2136/vzj2014.06.0077, 2014.

Ochsner, T., Cosh, M., Cuenca, R., Dorigo, W., Draper, C., Hagimoto, Y., Kerr, Y., Njoku, E., Small, E., and Zreda, M.: State of the art in large-scale soil moisture monitoring, Soil Sci. Soc. Am. J., 77, 1888, doi:10.2136/sssaj2013.03.0093, 2013.

Rosolem, R., Shuttleworth, W., Zreda, M., Franz, T., Zeng, X., and Kurc, S.: The effect of atmospheric water vapor on neutron count in the cosmic-ray soil moisture observing system, J. Hydrometeorol., 14, 1659–1671, doi:10.1175/JHM-D-12-0120.1, 2013.

Santa Regina, I., Tarazona, T., and Calvo, R.: Aboveground biomass in a beech forest and a Scots pine plantation in the Sierra de la Demanda area of northern Spain, Ann. Sci. Forest, 54, 261–269, doi:10.1051/forest:19970304, 1997.

Shuttleworth, J., Rosolem, R., Zreda, M., and Franz, T.: The COsmic-ray Soil Moisture Interaction Code (COSMIC) for use in data assimilation, Hydrol. Earth Syst. Sci., 17, 3205–3217, doi:10.5194/hess-17-3205-2013, 2013.

Rivera Villarreyes, C. A., Baroni, G., and Oswald, S. E.: Integral quantification of seasonal soil moisture changes in farmland by cosmic-ray neutrons, Hydrol. Earth Syst. Sci., 15, 3843–3859, doi:10.5194/hess-15-3843-2011, 2011.

Western, A., Zhou, S.-L., Grayson, R., McMahon, T., Blöschl, G., and Wilson, D.: Spatial correlation of soil moisture in small catchments and its relationship to dominant spatial, J. Hydrol., 286, 113–134, doi:10.1016/j.jhydrol.2003.09.014, 2004.

HESSD
12, 9813–9864, 2015

Zreda, M., Desilets, D., Ferré, T., and Scott, R.: Measuring soil moisture content non-invasively at intermediate spatial scale using cosmic-ray neutrons, Geophys. Res. Lett., 35, L21402, doi:10.1029/2008GL035655, 2008.

Zreda, M., Shuttleworth, W., Zeng, X., Zweck, C., Desilets, D., Franz, T., and Rosolem, R.: COSMOS: the COsmic-ray Soil Moisture Observing System, Hydrol. Earth Syst. Sc., 16, 4079–4099, doi:10.5194/hess-16-4079-2012, 2012.

HESSD

12, 9813–9864, 2015

Table 1. Overview of the five weighting and correction approaches for other than soil moisture effects on the CRS signal.

Approach	1 SDW	2 DSW	3 DDW	4 DDWnl	5 ABC
simple depth-weighting	yes	no	no	no	no
consideration of depth-specific W_L and SOM + B_R separately	no	yes	yes	yes	yes
distance depth-weighting	no	no	yes	yes	yes
non-linear depth-weighting	no	no	no	yes	no
consideration of above-ground biomass	no	no	no	no	yes

HESSD
12, 9813–9864, 2015

Table 2. Example of depth weighting (DSW) for a critical depth of $z^* = 22.1$ cm, $a = 0.0903$ and $b = 1$. Calibration campaign date 21 November 2014 (F4). Note the difference in specific weights if only soil water content θ is considered (wt(z,θ)) or if W_L and SOM + B_R is also considered (wt(z,H_p)).

Layer (cm)	θ (cm^3 cm^{-3})	W_L (cm^3 cm^{-3})	SOM + B_R (cm^3 cm^{-3})	H_p (cm^3 cm^{-3})	ρ_{bd} (g cm^{-3})
0–5	0.187	0.002	0.034	0.223	0.669
5–10	0.136	0.004	0.024	0.163	1.143
10–15	0.117	0.004	0.019	0.140	1.217
15–20	0.109	0.004	0.015	0.129	1.256
20–25	0.106	0.005	0.013	0.124	1.359
25–30	0.100	0.005	0.012	0.118	1.431

z(cm)	wt(z,θ)	$\int_z^{z+5}$wt(z,θ)	wt(z,H_p)	$\int_z^{z+5}$wt(z,H_p)
0	0.079	0.356	0.090	0.401
5	0.063	0.278	0.070	0.299
10	0.048	0.200	0.050	0.197
15	0.032	0.122	0.029	0.095
20	0.017	0.044	0.009	0.009
25	0.001	0.000	0.000	0.000
		$\Sigma = 1.00$		$\Sigma = 1.00$

HESSD
12, 9813–9864, 2015

Table 3. Atmospheric and soil parameters as well as neutron counts for the 10 calibrations. P is the atmospheric pressure, p_{v0} is the absolute humidity, N_{raw} is the raw neutron count, N_p is the pressure corrected neutron count, N_{pi} is the pressure and incoming radiation corrected neutron count, N_{pih} is the pressure, incoming radiation and water vapor corrected neutron count, N_0 is the calibration neutron count. N_{nm} is the incoming radiation from the neutron monitor, $\theta_{30\,cm}$ is the average soil moisture of the top 30 cm, θ_{depthW} is the depth-weighted soil moisture, $(W_L + SOM + B_R)_{depthW}$ is the depth-weighted sum of volumetric lattice water content, soil organic matter and root biomass water equivalent, $(H_p)_{depthW}$ is the depth-weighted hydrogen content of belowground hydrogen pools, $(\rho_{bd})_{depthW}$ is the depth-weighted bulk density and θ_{mod} is the average volumetric soil water content of the resulting time series using the N_0-calibration function (Desilets et al., 2010) with standard parameters. Mean (μ) and standard deviation (σ) values of the 10 calibration campaigns are given in the bottom lines.

Calibration	P (hPa)	p_{v0} (g m^{-3})	N_{raw} (n h^{-1})	N_p (n h^{-1})	N_{pi} (n h^{-1})	N_{pih} (n h^{-1})	N_0 (n h^{-1})
Winter	984.0	5.7	606.2	514.9	518.8	509.4	872.4
Spring1	999.3	8.6	549.2	523.0	527.5	526.2	868.7
Spring2	1021.0	4.9	491.1	550.6	542.8	530.5	871.1
Spring3	1002.9	9.6	544.7	533.1	539.9	541.5	869.2
Spring4	1019.0	8.0	503.4	556.0	549.4	546.1	879.0
Summer	1008.7	14.0	613.3	626.6	623.8	640.5	858.2
Fall1	998.7	11.5	624.7	592.4	593.8	601.5	909.5
Fall2	1014.1	7.8	509.3	542.1	546.7	542.8	876.2
Fall3	990.3	8.5	630.4	561.4	580.4	578.5	892.8
Fall4	1016.7	6.6	544.4	591.0	577.7	569.9	885.7
μ	1005.5	8.5	561.7	559.1	560.1	558.7	878.3
σ	11.9	2.6	50.2	33.1	31.1	37.5	13.8

insert line

HESSD
12, 9813–9864, 2015

Table 3. Continued.

Calibration	N_{nm} ($n\,h^{-1}$)	$\theta_{30\,cm}$ ($m^3\,m^{-3}$)	θ_{depthW} ($m^3\,m^{-3}$)	$(W_L + SOM + B_R)_{depthW}$ ($m^3\,m^{-3}$)	$(H_p)_{depthW}$ ($m^3\,m^{-3}$)	$(\rho_{bd})_{depthW}$ ($g\,cm^{-3}$)	θ_{mod} ($m^3\,m^{-3}$)
Winter	325.8	0.163	0.228	0.0343	0.262	0.985	0.141
Spring1	325.5	0.153	0.200	0.0340	0.234	1.013	0.143
Spring2	333.0	0.150	0.185	0.0311	0.216	0.955	0.137
Spring3	324.1	0.140	0.175	0.0324	0.207	1.000	0.143
Spring4	332.2	0.139	0.170	0.0302	0.200	0.957	0.145
Summer	329.8	0.073	0.080	0.0278	0.108	1.074	0.151
Fall1	327.4	0.112	0.137	0.0299	0.167	1.016	0.182
Fall2	325.5	0.140	0.174	0.0310	0.205	0.970	0.144
Fall3	317.5	0.119	0.149	0.0316	0.181	1.018	0.166
Fall4	335.8	0.126	0.150	0.0293	0.179	0.981	0.155
μ	327.7	0.131	0.165	0.0312	0.196	0.997	0.151
σ	5.0	0.024	0.038	0.0019	0.039	0.034	0.013

HESSD
12, 9813–9864, 2015

Table 4. Mean (μ) and standard deviations (σ) of calibration parameter N_0 and resulting time series of volumetric soil water content θ_{mod} for the five approaches with 10 calibration campaigns each.

Approach	$(N_0)_\mu$ (n h^{-1})	$(N_0)_\sigma$ (n h^{-1})	$(\theta_{mod})_\mu$ (m^3 m^{-3})	$(\theta_{mod})_\sigma$ (m^3 m^{-3})
1 SDW	855.0	17.3	0.158	0.015
2 DSW	878.3	13.8	0.151	0.013
3 DDW	841.0	21.5	0.138	0.017
4 DDWnl	827.7	19.4	0.133	0.016
5 ABC	1970.9	50.4	0.138	0.017

HESSD
12, 9813–9864, 2015

Table 5. New calibration parameters for the five approaches.

	N_0	a_0	a_1	a_2
1 SDW	926.3	0.203	0.109	0.238
2 DSW	1007.8	0.203	0.114	0.267
3 DDW	814.7	0.328	0.001	0.311
4 DDWnl	904.3	0.272	0.000	0.283
5 ABC	1249.1	0.502	0.001	0.312

HESSD
12, 9813–9864, 2015

Table 6. Performance measures for the five approaches – comparison of new calibration with standard calibration (SD). KGE' is the modified Kling–Gupta efficiency, β is the bias ratio and γ is the variability ratio. μ KGE' and σ KGE' represent the mean and standard deviation of the KGE' values of the 10 individual single-point standard calibrations.

	KGE' new	β new	γ new	μ KGE' SD	σ KGE' SD	μ β SD	μ γ SD
1 SDW	0.830	0.849	0.986	0.675	0.045	1.120	1.258
2 DSW	0.880	0.915	0.964	0.727	0.035	1.032	1.231
3 DDW	0.921	1.018	1.006	0.676	0.087	0.887	1.258
4 DDWnl	0.871	1.090	1.051	0.674	0.107	0.828	1.246
5 ABC	0.920	1.025	0.999	0.676	0.087	0.887	1.258

HESSD
12, 9813–9864, 2015

Figure 1. Field site location in Müritz National Park in north-eastern Germany.

HESSD
12, 9813–9864, 2015

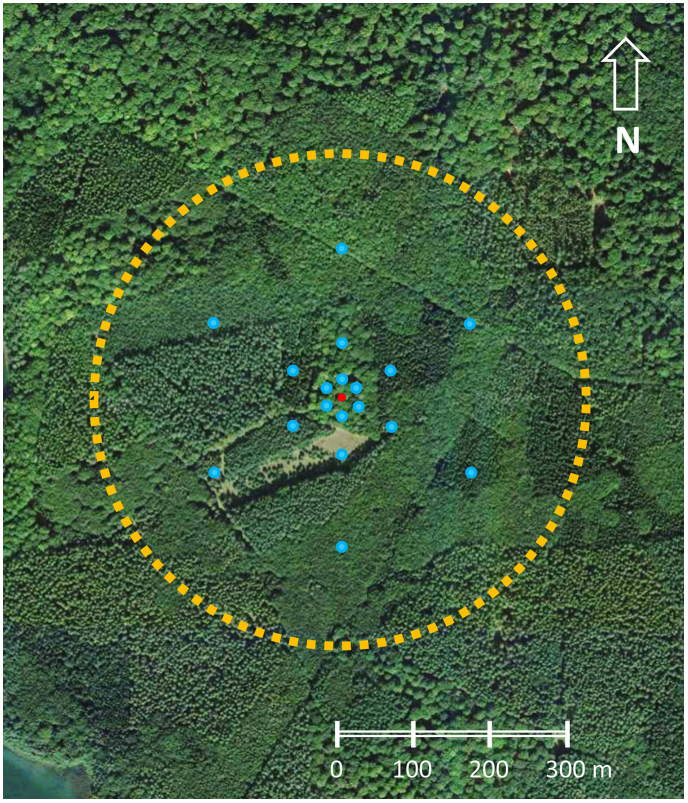

Figure 2. Soil sampling locations for calibration (blue dots) and forest vegetation around the CRS (red dot in the center). The TDT soil moisture sensors are located in close vicinity to the sampling locations. The yellow circle approximates the footprint of the CRS (diameter = 300 m).

HESSD
12, 9813–9864, 2015

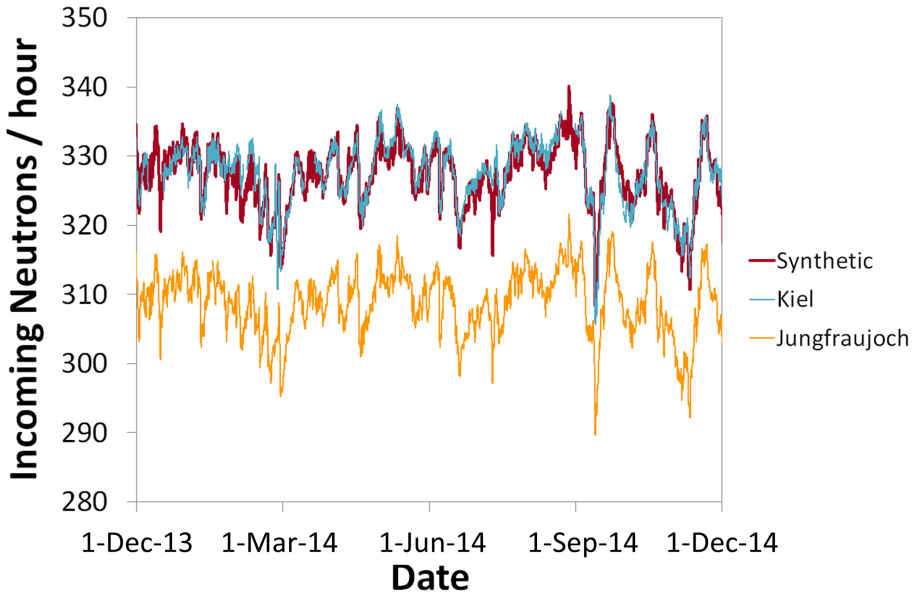

Figure 3. Incoming neutron flux from the neutron monitors in Kiel, Germany and Jungfraujoch, Switzerland and synthetic continuous time series of incoming neutron flux combined from these two and used for the corrections in this study.

HESSD
12, 9813–9864, 2015

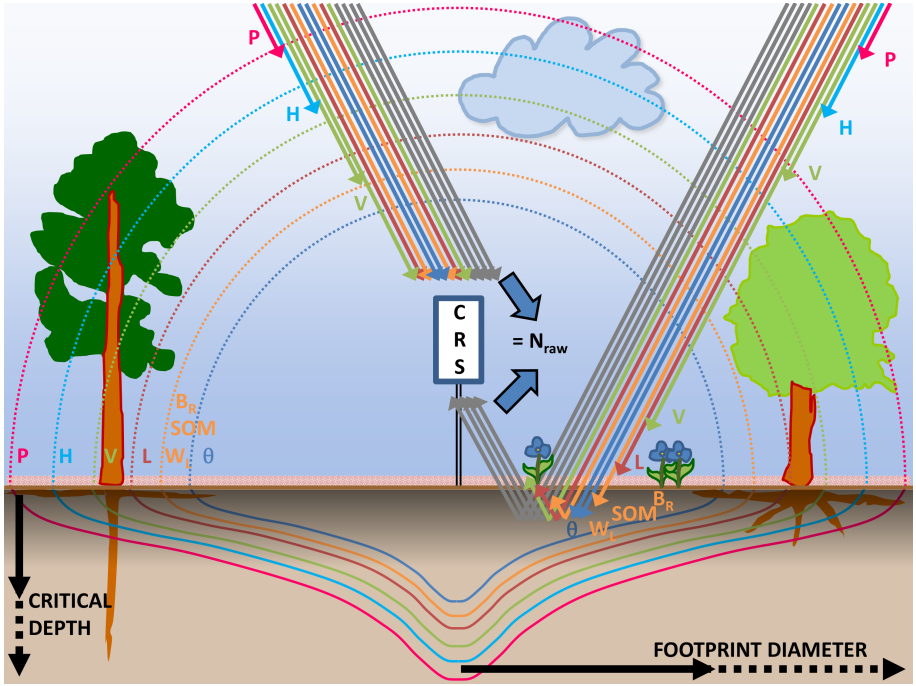

Figure 4. Factors influencing the raw neutron count (N_{raw}) and the measurement support of the CRS in terms of critical depth and footprint. Barometric pressure (P), air humidity (H), vegetation (V), litter layer (L), soil organic matter (SOM), root biomass (B_R) and lattice water (W_L) need to be accounted for to isolate the signal from soil water content (θ).

HESSD
12, 9813–9864, 2015

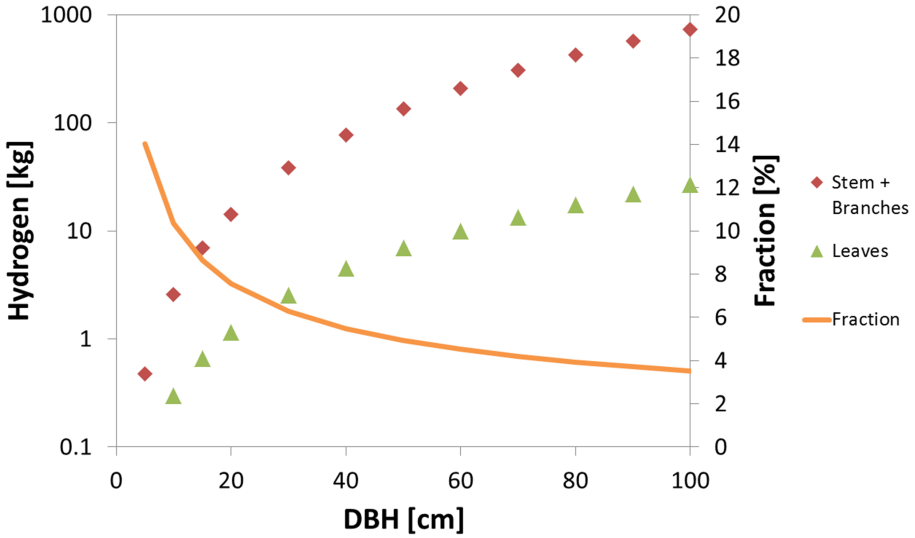

Figure 5. Mass of hydrogen in individual beech trees in stem and branches (red diamonds) and leaves (green triangles) in relation to diameter at breast height (DBH). Fraction of leaf hydrogen mass of total aboveground tree hydrogen mass (orange line).

HESSD
12, 9813–9864, 2015

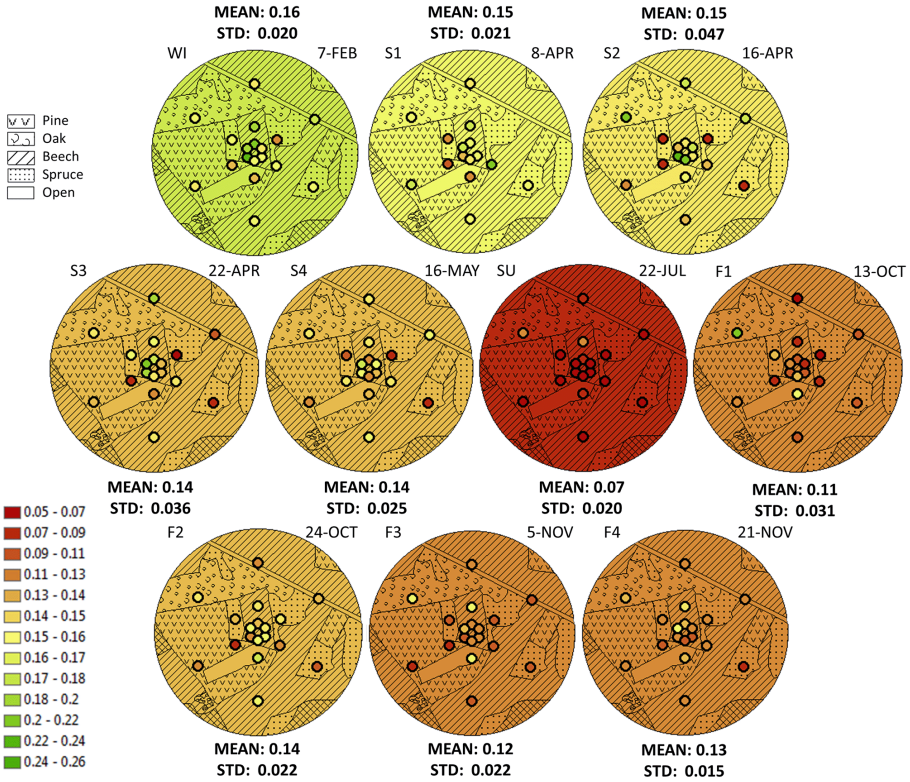

Figure 6. Gravimetrically determined volumetric soil water content patterns in the footprint of the CRS for the 10 calibration dates. The colored dots indicate the unweighted average value from 0 to 30 cm at the 18 calibration locations. Background colors represent the unweighted average value of all 108 soil samples. Different forest stands (pine, beech, oak, spruce) are indicated by the patterned background.

HESSD
12, 9813–9864, 2015

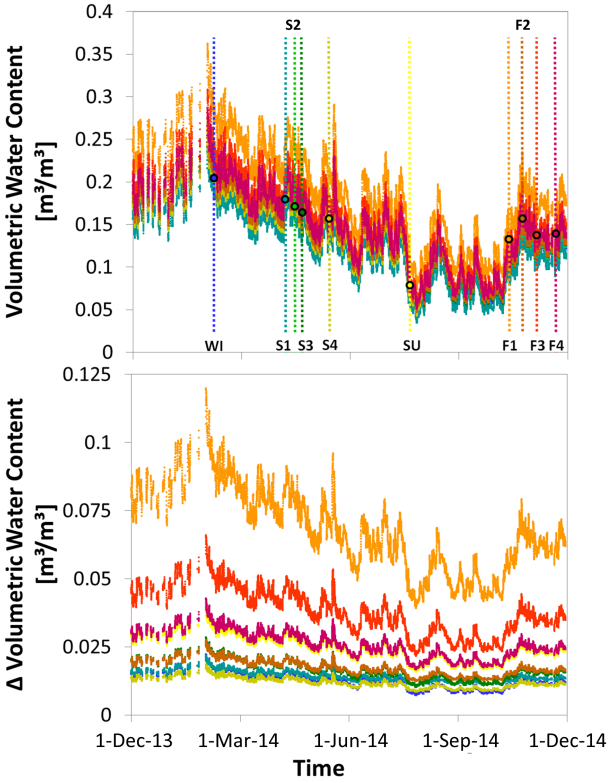

Figure 7. Upper panel: volumetric water content derived from CRS data for the 10 calibration dates (vertical lines, colors correspond to time series colors). Filled circles represent the depth-weighted volumetric water content at the time of calibration (according to DSW). Lower panel: differences in water content between the calibration resulting in the driest time series (S2) and all other calibrations.

HESSD
12, 9813–9864, 2015

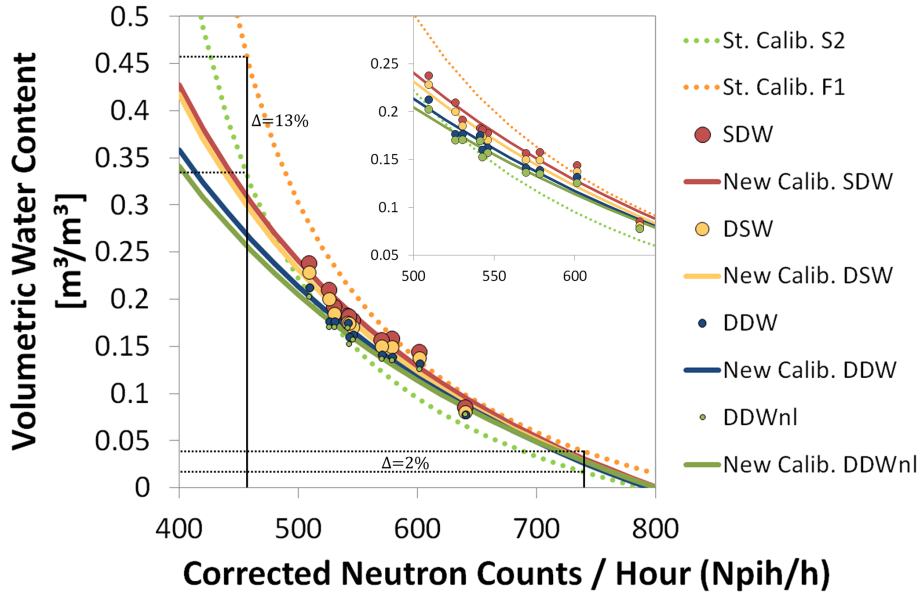

Figure 8. New calibration functions (solid lines) for the four different weighting approaches (simple depth-weighting SDW, depth-specific weighting DSW, distance–depth-weighting DDW, distance–depth-weighting, non-linear DDWnl), each one derived from 10 calibration points (circles). Calibration points are better captured by flatter calibration functions (solid lines) with new calibration parameters than by any of the standard calibration functions (dotted lines) based on a single calibration data set only (days S2 and F1 as an example). Black lines illustrate that differences in soil moisture between the results of individual calibrations are larger when soil moisture is high. The inset magnifies the area around the calibration points.

HESSD
12, 9813–9864, 2015

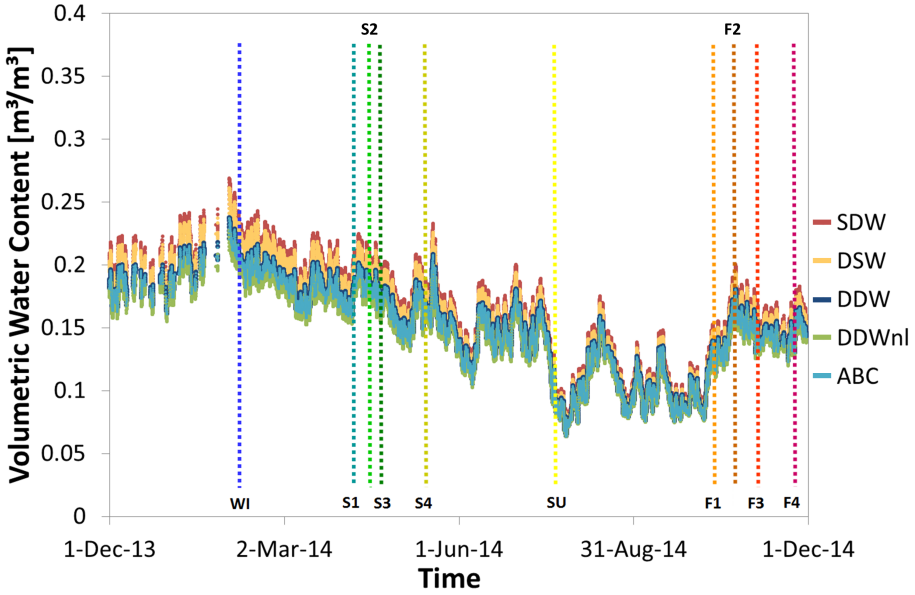

Figure 9. Time series of volumetric water content derived with new calibration functions with new calibration parameters based on the five calibration approaches: simple depth-weighting (SDW), depth-specific weighting (DSW), distance–depth-weighting (DDW), distance–depth-weighting, non-linear (DDWnl) and aboveground biomass correction (ABC).

HESSD
12, 9813–9864, 2015

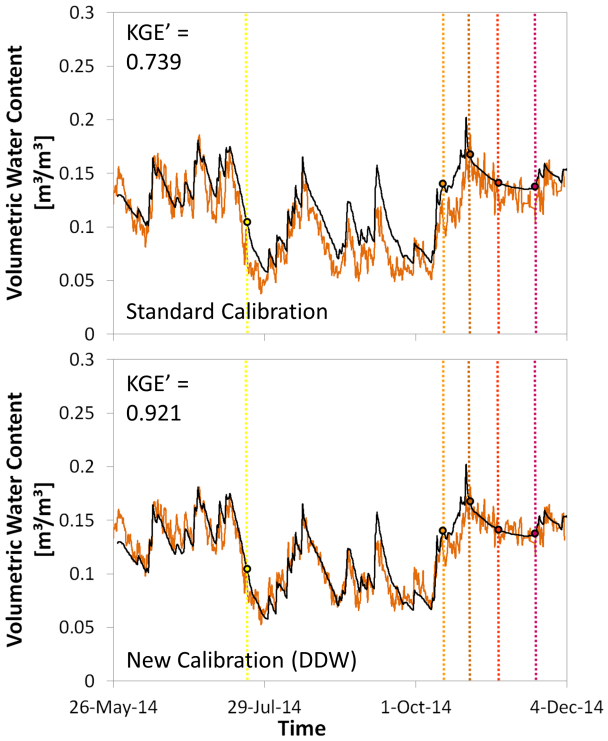

Figure 10. Volumetric water content derived from TDT measurements (black line) and CRS measurements (orange line) using different calibration functions. Upper panel: the orange line is an average of the volumetric water content derived from the 10 calibration campaigns of the CRS using the standard N_0-calibration function from Desilets et al. (2010) applying the DDW weighting approach. Lower panel: the orange line is the volumetric water content derived from a new calibration function with modified calibration parameters applying the DDW weighting approach. The colored vertical lines mark the days of the last five calibration campaigns.

HESSD
12, 9813–9864, 2015

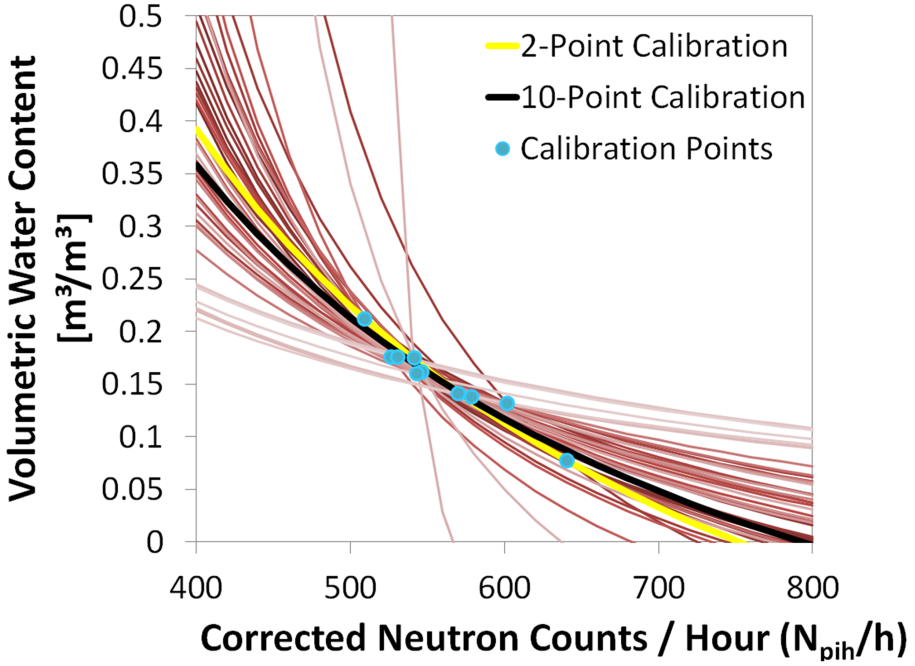

Figure 11. Best-fit N_0-calibration functions (red-brown colored lines) for all combinations of two-point calibrations (blue dots). Best-fit N_0-calibration function for 10-point calibration (black line). Best-fit two-point N_0-calibration function derived from calibration points with highest and lowest volumetric water content (yellow line).

HESSD
12, 9813–9864, 2015

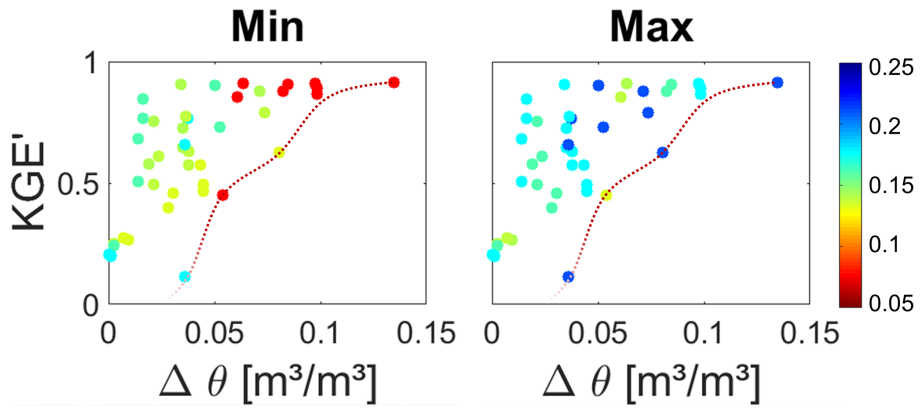

Figure 12. Performance of CRS soil water content data derived from two-point calibrations in relation to distance between soil moisture states at the two calibration dates. The color bar indicates volumetric soil water content. Left panel: points are colored according to the soil water content of the drier calibration date. Right panel: points are colored according to the soil water content of the wetter calibration date. Dashed lines: Pareto front indicating that soil moisture differences of less than 0.1 $m^3\,m^{-3}$ can produce N_0-calibration curves with sub-optimal conversions of neutron counts to volumetric soil water content.

HESSD
12, 9813–9864, 2015